Simultaneous Fat Saturation and Magnetization Transfer Contrast Imaging with Steady-State Incoherent Sequences

Feng Zhao,[1]* Jon-Fredrik Nielsen,[1] Scott D. Swanson,[2] Jeffrey A. Fessler,[3] and Douglas C. Noll[1]

Purpose: This work combines an *n*-dimensional fat sat(uration) radiofrequency (RF) pulse with steady-state incoherent (SSI) pulse sequences, e.g., spoiled gradient-echo sequence, to simultaneously produce B_0 insensitive fat suppression and magnetization transfer (MT) contrast. This pulse is then referred to as "fat sat and MT contrast pulse."

Theory: We discuss the features of the fat sat and MT contrast pulse and the MT sensitivities of the SSI sequences when combining with fat sat. Moreover, we also introduce an adapted RF spoiling scheme for SSI sequences with fat sat. Methods: Simulations and phantom experiments were conducted to demonstrate the adapted RF spoiling. Fat suppression and MT effects are shown in 3T phantom experiments and in vivo experiments, including brain imaging, cartilage imaging, and angiography.

Results: To ensure that the sequence reaches steady state, the adapted RF spoiling is required for fat sat SSI sequences. Fat sat and MT contrast pulse works robustly with field inhomogeneity and also produces MT contrasts.

Conclusion: SSI sequences with fat sat and MT contrast pulse and adapted RF spoiling can robustly produce fat suppressed and MT contrast images in the presence of field inhomogeneity. **Magn Reson Med 74:739–746, 2015. © 2014 Wiley Periodicals, Inc.**

Key words: fat saturation; magnetization transfer; pulse design; spectral-spatial pulse; RF spoiling; field inhomogeneity

INTRODUCTION

Effective fat suppression or separation is critical for diagnostic quality in body MRI and is commonly used to eliminate undesired adipose tissue signals or prevent chemical shift artifacts. Fat sat(uration) is one popular fat suppression technique that uses a spectrally selective pulse to selectively saturate and dephase fat spins preceding the actual imaging pulse sequence (1). Fat sat typically works well and is compatible with most imaging sequences, but it is sensitive to B_0 and B_1 inhomogeneity. Moreover, the fat sat pulse is long in low field scanners, limiting the minimum T_R for some fast MRI sequences. These problems have been mitigated using a 4D tailored spectral-spatial fat sat pulse proposed in (2). That fat sat pulse is robust to B_0/B_1 inhomogeneity and more time-efficient than the standard fat sat pulse.

Magnetization transfer (MT) is often used to increase vessel contrast in MR angiography (MRA) (3) and to indirectly image semisolid components of tissue, such as collagen (4) or myelin (5). Protons in these semisolids have a very broad spectrum and can be selectively saturated by off-resonance radiofrequency (RF) pulses. MT effect is then generated by magnetic exchange between the immobilized components in tissue (proteins, polysaccharides, or lipid bilayers) and the detected water protons. Using this tissue-dependent feature, magnetization transfer contrast (MTC) sequences can produce MTC images with useful diagnostic information. MTC imaging applies the MT pulse either only once prior to the steady-state imaging sequence (6) (turbo MT preparation) or in every repetition (7); in this article, we focus on the latter approach because it shows higher MT sensitivity and thus less specific absorption rate penalty when T_R is short.

Combining fat sat and MTC is beneficial in many clinical applications, such as cartilage imaging (7,8), cardiac imaging (6), intracranial angiography (3), breast imaging (9), and lung imaging (10). In angiography applications, spoiled gradient-echo sequence (SPGR) has been widely used to produce T_1-weighted or flow-enhanced images with very short imaging times, e.g., time-of-flight angiography (6). SPGR belongs to the class of "steady-state incoherent (SSI) sequences" that eliminate residual transverse magnetization prior to each RF pulse (11). SSI sequences are usually compatible with using fat sat and MT pulses applied in each repetition. In applications that need more T_2 weighting, e.g., MTC cartilage imaging, the balanced steady-state free precession sequence is a preferred fast imaging sequence that produces high signal-to-noise ratio (SNR) T_2/T_1 contrast images. However, a drawback of balanced steady-state free precession sequence is the banding artifacts caused by B_0 field inhomogeneity, and it belongs to "steady-state coherent (SSC) sequences" (11) that have limited compatibility with fat sat and MT pulses in each repetition. Nielsen et al. (12,13) proposed an SSI sequence called "small-tip fast recovery (STFR)" that produces balanced steady-state free precession sequence-like high SNR T_2/T_1 contrast images that are free of banding artifacts.

Although SSI sequences like SPGR or STFR allow using fat sat and MT pulses in each repetition, some limitations may hamper their practical use. Combining both

[1]Biomedical Engineering Department, The University of Michigan, Ann Arbor, Michigan, USA.
[2]Radiology Department, The University of Michigan, Ann Arbor, Michigan, USA.
[3]Department of Electrical Engineering and Computer Science, The University of Michigan, Ann Arbor, Michigan, USA.
Grant sponsor: National Institutes of Health; Grant numbers: R01NS058576 and R21EB012674.
*Correspondence to: Feng Zhao, Ph.D., 5 Technology Drive, Milpitas, CA 95035. E-mail: zhaofll@umich.edu
Additional Supporting Information may be found in the online version of this article.
Received 8 April 2014; revised 1 September 2014; accepted 4 September 2014
DOI 10.1002/mrm.25475
Published online 22 September 2014 in Wiley Online Library (wileyonlinelibrary.com).

fat sat and MT pulse into one sequence may increase minimal T_R too much for practical use in applications like breath-hold imaging, especially at low fields. In addition, such combinations may generate specific absorption rate problems at high fields.

In this work, we propose to apply the n-dimensional tailored spectral-spatial fat sat pulse proposed in (2) to SSI sequences, including SPGR and STFR, to produce fat suppressed MTC images. In the context of this article, such pulse is referred to as "fat sat and MT contrast pulse" (FSMT-pulse). The major contribution of this work is the combination of FSMT-pulse and SSI sequences. FSMT-pulse has short pulse length and very high power efficiency (2). Its pulse length mitigates the issue of limited T_R in steady-state imaging, and the high power efficiency contributes to MT contrasts. The other contributor to MT contrasts is the fat-sat SSI sequence itself, which has high sensitivity to MT. The issue of limited T_R is further mitigated by the fact that no special MT pulse is needed. In addition, the FSMT-pulse is also robust to B_0/B_1 inhomogeneity, mitigating a general problem in fat sat imaging. Furthermore, we found that the conventional RF spoiling scheme that is typically used for SPGR and STFR does not always work when pulses with crushers like fat sat are applied, so we introduce an adapted RF spoiling scheme for the proposed sequences.

In this article, we demonstrate the proposed methods with simulation studies, phantom experiments and in vivo experiments like human brain imaging, cartilage imaging, and time-of-flight-based MRA at 3T. Because we had very similar conclusions for the two SSI sequences, i.e., SPGR and STFR, we focus on the proposed SPGR sequence in the rest of the article. The studies of the proposed STFR sequence are shown in the Supporting Information.

THEORY

SPGR With FSMT-Pulse

Figure 1 illustrates the 2D version of the proposed fat sat and MTC SPGR (FSMT-SPGR) sequence. The fat sat and MT part (S_1) with the FSMT-pulse (P_0) is added prior to the regular excitation pulse (P_1) of SPGR (S_2) in each repetition, and both S_1 and S_2 have a gradient crusher, i.e., C_1 and C_2. This 2D version of FSMT-SPGR uses a 3D FSMT-pulse (14,15) that is tailored to the B_0/B_1 field using the same method proposed in (2), and it uses repeated 2D spiral-out trajectories to cover the 3D spectral-spatial k-space (14,15). The 3D version of the FSMT-SPGR uses the same FSMT-pulse used in (2). The key features of the FSMT-pulse mentioned in (2) include robustness to field inhomogeneity and shorter pulse lengths. By traversing multidimensional spectral and spatial excitatoin k-space very efficiently, FSMT-pulse has much higher power efficiency, e.g., up to 60–100 times, than the regular spectral-select fat sat pulse at 3T (2). This feature contributes to the MT contrast discussed in the next section. In addition, these concise pulse sequences mitigate the issue of limited T_R in steady-state imaging.

Simultaneous Fat Sat and MTC Imaging

For a given MT pulse, SPGR with the MT pulse applied in each repetition produces higher MT effects than the one with the turbo type MT prep. Defining MT ratio (MTR) as the ratio between the amount of magnetization reduced by MT and the original magnetization, the Appendix shows that the steady-state longitudinal magnetization of MTC SPGR prior to each P_1 with respect to MTR is:

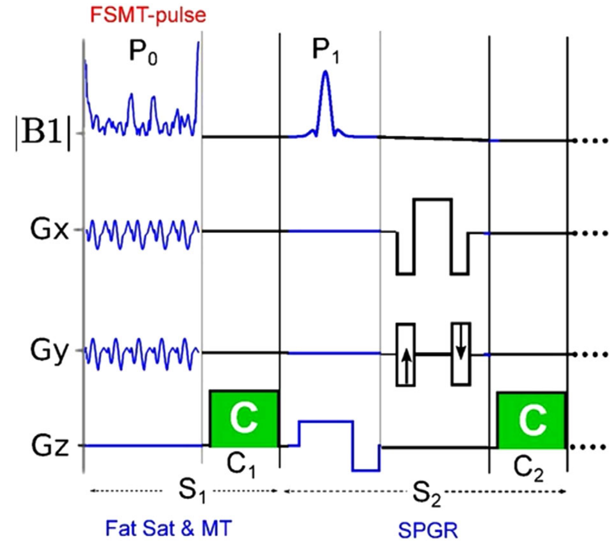

FIG. 1. Illustration of the 2D version of the proposed FSMT-SPGR sequence.

$$M_z(\mathrm{MTR}) = M_0 \frac{(1-\mathrm{MTR})E_{1s}(1-E_{1d}) + (1-E_{1s})}{1-(1-\mathrm{MTR})E_{1s}E_{1d}\cos\alpha} \qquad [1]$$

where M_0 is equilibrium magnetization, $E_{1s} \triangleq e^{-\frac{T_s}{T_1}}, E_1 \triangleq e^{-\frac{T_d}{T_1}}$, T_s is the duration of each gradient crusher, T_d is the duration of each repetition excluding the MT part, α is the flip angle, relaxation during the MT pulse is ignored.

To show that MTC SPGR is more efficient in producing MT effects than the turbo MT-prep sequences, Figure 2 shows curves of $1 - M_z(\mathrm{MTR})/M_z(0)$ for ranges of T_1 and T_2 values, where $1 - M_z(\mathrm{MTR})/M_z(0)$ is the "effective MTR" of SPGR. Note that MTR defined above is not necessarily equal to effective MTR, as MTR reflects only the magnetization change caused by the MT pulse, while the effective MTR represents the steady-state magnetization change, which is a combined effect of the MT pulse and the steady-state sequence. The simulation was run with $T_d = 10$ ms and $T_s = 1$ ms. Note that MTR is equal to the effective MTR of the turbo MT prep sequences, so the plots show that with reasonable T_1 and T_2 values, MTC SPGR with MT pulses applied in each repetition are much more efficient in producing MT effects than the corresponding turbo MT prep sequence. Such MT sensitivity increases with shorter T_R or longer T_1 and does not change much with different T_2 values.

With this property, we propose to use SPGR with FSMT-pulse to generate MT effect and suppress fat simultaneously. Although SPGR is MT sensitive, SPGR with the conventional spectrally selective fat sat pulse produces too little MT effect for clinical use, because the conventional fat sat pulses are low energy pulses

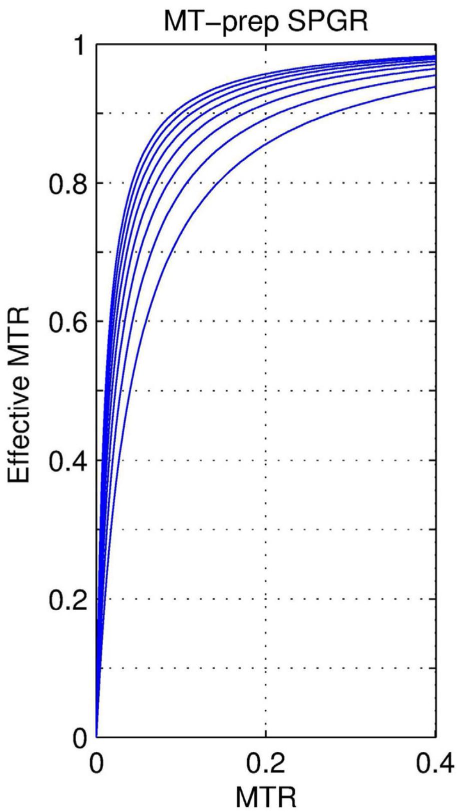

FIG. 2. Plots of the effective MTR in terms of MTR for MTC SPGR; the plots are from all the combinations of the following relaxation parameters: $T_1 = [0.5, 0.7, \ldots, 1.7, 1.9]$ s and $T_2 = [50, 70, \ldots, 170, 190]$ms. As the curves do not change much with different T_2 values, the curves are in eight bundles corresponding to eight T_1 values. SPGR is sensitive to small magnetization attenuation caused by MT effect.

compared to typical MT pulses (6) and MT effects increase with RF energy (16). However, the proposed FSMT-pulse produces much higher RF energy than the conventional fat sat pulse, because this short efficient tailored spectral-spatial pulse needs to handle both spectral and spatial variations by traversing the excitation k-space very rapidly, leading to higher RF amplitude and thus higher RF energy (2). In addition, the FSMT-pulse is about 3.5 ppm off the center frequency, which is much lower than the off-resonance frequency of the conventional MT pulses. This can further increase the MT effects induced by the FSMT-pulse, as MT effects decrease with off-resonance frequency (16). Thus, the proposed FSMT-pulse can potentially produce useful MT effects while suppressing fat signal.

In practice, it is hard to separate MT effects and direct water spectrum excitation caused by fat sat pulse. Direct excitation to water causes the same effects as if there were MT effects. Thus, the property shown in Figure 2 also indicates that these sequences are very sensitive to direct excitation of water by imperfect FSMT-pulse or Shinnar-Le Roux (SLR) fat sat pulses in the presence of field inhomogeneity. Such direct water excitation should be minimized to avoid confusion with MT effects. We observed significant signal drop in MT-free materials when using a SLR pulse that has ripples in the water band smaller than 5% of the fat band amplitude, which is consistent to Figure 2. Thus, the SLR fat sat pulse used in our experiments was designed with very strict restriction on the amplitude of ripples around the water spectrum. Similarly, the FSMT-pulse design also needs to fit the target pattern of the water bands very strictly. In contrast, these sequences are not so sensitive to inaccurate fat suppression, so the FSMT-pulse design allows less accurate fat band fitting to accommodate the high demands in water bands. Specifically, we set the bandwidths of water much wider than the corresponding fat bandwidths in the pulse design.

Adapted RF Spoiling Scheme

Conventional SPGR without fat sat needs gradient crushers to spoil the residual transverse magnetization before the next imaging cycle, and RF spoiling is also required when $T_R < T_2$ (12,17). RF spoiling removes the residual transverse signal by quadratically varying the global RF phase, producing incoherent intra-voxel spin behaviors. In SPGR without fat sat, the global phase of P_1 varies as the following quadratic function (17):

$$\Phi_{P_1}(n) = \frac{a}{2}n^2 + bn + c \qquad [2]$$

where a, b, c are constants, and n is the number of repetitions. The quadratically changing phase guarantees that the signal of each voxel reaches a homogeneous steady state, and the residual transverse magnetization at the end of each repetition can be kept to almost zero by choosing a particular value of a, for example, 117°.

However, sequences with additional crushers in each repetition, e.g., fat sat sequences, may not work robustly with the conventional RF spoiling scheme, i.e., P_0 keeps the same global phase as P_1. For SPGR with fat sat, conventional RF spoiling scheme needs perfect fat sat to guarantees that the signals reach steady state. In this ideal situation, water or fat experiences only one RF pulse, i.e., P_1 or P_0, in each repetition. However, fat sat is imperfect in practice. When using conventional fat sat, even if the B_0 inhomogeneity is not severe enough to have water excited by the fat sat pulse, fat signals can never be perfectly eliminated in the presence of B_0/B_1 inhomogeneity; then fat spins can be excited both by P_0 and P_1, and the additional crusher C_1 will alter the signal's progression to steady state. Although the FSMT-pulse can greatly improve fat sat in the presence of B_0/B_1 inhomogeneity, it still can not work perfectly.

To improve robustness of SPGR with fat sat, we propose to adapt the conventional RF spoiling scheme to better approach steady state with imperfect fat sat. The new RF spoiling scheme applies the quadratic RF phase variation to each "sub-unit that contains a crusher" instead of to each repetition. We use the following global phase of each pulse in SPGR with fat sat:

$$\begin{aligned} \Phi_{P_0}(n) &= \frac{a}{2}(2n-1)^2 + b(2n-1) + c \\ \Phi_{P_1}(n) &= \frac{a}{2}(2n)^2 + b(2n) + c \end{aligned} \qquad [3]$$

If the two crushers C_1 and C_2 have the same area, this adapted RF spoiling ensures that the sequence reaches steady state (17).

Furthermore, one must properly choose the parameter a in (3) to completely remove the remnant transverse magnetization at the end of each repetition. We empirically chose $a = 117°$ for all our experiments based on simulations and some phantom experiments. There are also other good values for the fat sat SPGR with the adapted RF spoiling, such as 74°. When B_0 map is close to uniform, the transverse magnetization of most spins experience only one crusher in each repetition, and then, the sequence would almost work as the conventional RF spoiling but with four times linear phase increments. In this case, $a = 117°/4$ may be a good choice.

METHODS

Simulation and Phantom Experiment I: RF Spoiling Schemes

We first compared the conventional RF spoiling scheme and the adapted RF spoiling scheme by Bloch equation simulations. We simulated the signal evolutions of the integrated magnetization of a 0.5 cm voxel with 5000 equally-spaced isochromats for fat or water with fat sat SPGR. We chose some typical values for the fat spin and the water spin: $T_{1,\text{fat}}/T_{2,\text{fat}} = 200$ ms/70 ms, $T_{1,\text{water}}/T_{2,\text{water}} = 1$ s/100 ms; the sequence parameters were: $T_R = 10$ ms, the tip angle of P_1 was 20° for both water and fat, the tip angle of P_0 was 80° for fat and 20° for water to simulate imperfect fat sat, and the parameter a in (2) and (3) was 117°. We simulated evolutions of the transverse magnetization of fat and water right after P_1 for the first 200 and 500 repetitions (2 s and 5 s), respectively, which were sufficient to test whether the signals reach steady state.

In addition, we also applied fat sat SPGR in a phantom scan on a 3T GE scanner (GE Healthcare, Milwaukee, WI). The phantom was a cylindrical phantom filled with distilled water and vegetable oil. The fat sat part used a conventional spectrally selective fat sat pulse designed by the SLR algorithm (18). The SLR fat sat pulse is 5-ms long and has a 400 Hz minimal phase passband for fat (center frequency is −435 Hz), which is a standard setting for 3T fat sat. With this fat sat pulse, a 3D SPGR with spin-warp readout was applied using the conventional and the adapted RF spoiling schemes respectively, and the imaging parameters were: $T_R = 13$ ms, field-of-view (FOV) = 14 × 14 × 14 cm^3, data size = 64 × 64 × 14, $a = 117°$. A set of images without fat sat also were acquired for reference.

Phantom Experiment II: Fat Sat Pulses

The FSMT-pulse used for 3D or multislice imaging has been demonstrated in (2). In our experiments with FSMT-SPGR sequences, we also performed 2D scans that need only a 3D version of the FSMT-pulse. Phantom experiments were performed at 3T to test 2D SPGR sequences with 3D FSMT-pulse. The phantom was the same cylindrical water/oil phantom used in the previous experiment. Similar to (2), we designed each 3D FSMT-pulse using only a 2D B_0 field map, assuming that B_1 homogeneity is acceptable in our single channel excitation experiments. These FSMT-pulses were compared with the 5 ms SLR fat sat pulse used in the previous experiment. The goal of this study was to demonstrate that SPGR with 3D FSMT-pulse is more robust to B_0 inhomogeneity than using the SLR fat sat pulse.

The sequence was applied to different slices of the phantom to acquire multiple 2D axial slice images, where each FSMT-pulse was designed using the corresponding 2D B_0 map. We acquired B_0 maps from two gradient-echo images with different echo times, and the echo time difference had water and fat spins in-phase, e.g., $\Delta T_E = 2.272$ ms at 3T, to eliminate the phase difference caused by chemical shift. All the FSMT-pulses, which were only 2.1 ms long, used five repetitions of 2D spiral-out excitation k-space trajectories, and the adapted RF spoiling scheme (3) was applied to those sequences. All the data were acquired with 2D spin-warp k-space trajectories, and the imaging parameters of the SPGR sequences were: FOV = 14 × 14 cm^2, slice thickness = 6 mm, data size = 64 × 64, $a = 117°$, and $T_R = 11.6$ ms, and 14.5 ms for the sequence with the 2.1 ms FSMT-pulse and the 5 ms SLR fat sat pulse, respectively. For each fat suppressed image, we also acquired its corresponding non-fat-suppressed image with the fat sat pulse turned off.

Phantom Experiment III: Simultaneous Fat Sat and MTC Imaging

To test MT effects, we made a special cylindrical MT phantom filled with mixture of Prolipid 161 (Ashland Specialty Ingredients) and $NiCl_2$ solution. The material has similar T_1, T_2, and MT values to white matter at 3T. In addition, we made a spherical phantom filled with mineral oil and distilled water doped with $MnCl_2$, and the $MnCl_2$ solution was carefully tuned to match the T_1 and T_2 values of the MT phantom material at 3T. To test the effect of simultaneous fat sat and MTC, we put both phantoms in one field of view and applied the proposed FSMT-SPGR on the 3T scanner. Similar to the previous phantom experiment, we first acquired a 2D B_0 map, and then designed the FSMT-pulse based on the field map. FOV of the field map used in the design was 18 cm × 18 cm, and the pulse length was increased to 2.7 ms with seven repetitions of spiral-out trajectories to accommodate the B_0 field that has big variations between the two phantoms (Fig. 6). 2D spin-warp readouts were applied to the same part of the object with the FSMT part on or off, and the imaging parameters were: FOV = 18 × 18 cm^2, slice thickness = 6 mm, data size = 64 × 64, $a = 117°$, and $T_R = 16$ ms.

In-Vivo Experiments I: Simultaneous Fat Sat and MTC Imaging in Brain

We tested the proposed FSMT-SPGR in an in vivo experiment on the 3T GE scanner, where we scanned axial brain slices of a healthy subject. Similar to the phantom experiments, 2D B_0 maps were first acquired for the FSMT-pulse design. The FSMT-pulse was 2.3-ms long with seven repetitions of 2D spiral-out trajectories. Two-dimensional spin-warp readout was used to acquire an axial slice around the level of eyes, where the designed FSMT part was on or off, respectively. The imaging parameters were: FOV = 24 × 24 cm^2, slice thickness = 6 mm, data size = 256 × 256, $a = 117°$, and $T_R = 15.3$ ms.

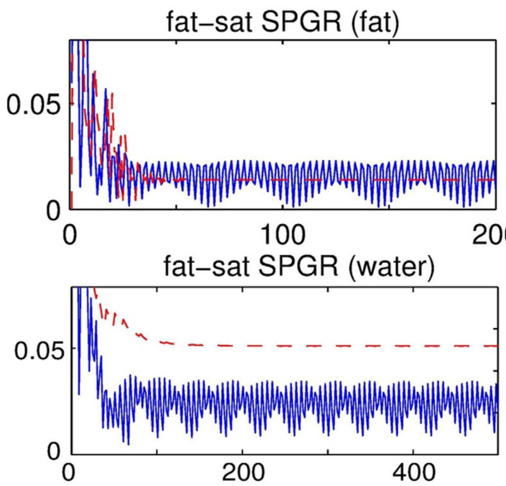

FIG. 3. Signal evolutions of fat spin (upper row) and water spin (lower row) using fat sat SPGR with different RF spoiling schemes. Both vertical axes denote the ratio between the transverse magnetization right after P_1 and the magnetization at equilibrium, M_{xy}/M_0; the horizontal axes denote the number of repetitions. The signal reaches steady state with the adapted RF spoiling scheme (dashed lines) but not with the conventional RF spoiling scheme (solid lines).

In-Vivo Experiments II: MRA in Brain

Lastly, we applied the proposed FSMT-SPGR to MRA in human cerebral arteries where fat suppression and MT can help suppress surrounding fat and other background tissue, respectively. We acquired 3D time-of-flight images over a 4-cm thick axial slab around the circle of Willis with a 3D SPGR sequence. In addition, FSMT-pulse was designed based on the 3D B_0 map of an extended 3D axial slab that covered the imaging slab and its adjacent inferior axial slab (4-cm thick). By designing for this extended volume, direct excitation of the arterial blood in the upstream region by the FSMT-pulse can be largely reduced, because the FSMT-pulse has unpredictable effects to out-of-ROI regions. The FSMT-pulse was 2.5-ms long using a repeated 3D spiral trajectory (2,19). The image data were acquired with 3D spin-warp readout, and two sets of images were taken with the proposed FSMT part on or off respectively. The imaging parameters were: $T_E = 3.28$ ms, $T_R = 11.4$ ms, flip angle $= 20°$, $a = 117°$, $0.94 \times 0.94 \times 2$ mm^3 resolution, FOV $= 24 \times 24 \times 4$ cm^3.

RESULTS

Simulation and Phantom Experiment I: RF Spoiling Schemes

Figure 3 shows the signal evolutions of fat or water when fat sat SPGR is applied with the conventional RF spoiling scheme or the adapted RF spoiling scheme. In all the plots, the sequence with the conventional RF spoiling scheme did not reach steady state (blue solid lines), but the one with the adapted RF spoiling scheme reached steady state after 100 repetitions at most (red dashed lines). With the signal oscillating over repetitions, the data of the conventional RF spoiling scheme are inconsistent in the k-space, causing ghosting artifacts. This is shown in Figure 4 where the image acquired with the conventional RF spoiling scheme has ghosting artifacts along the phase-encoding direction of the spin-warp trajectory, while the one with the adapted RF spoiling scheme shows a fat-suppressed image free of ghosting artifacts.

Phantom Experiment II: Fat Sat Pulses

Figure 5 shows the resulting images produced by the SPGR sequences and the corresponding B_0 maps. The original images without fat sat are in the first column, the B_0 maps are in the second column, and the ratio images by the FSMT-pulse and the SLR fat sat are shown in the third and fourth columns, respectively. The ratio image is calculated by taking the ratio between the image with fat sat and the corresponding image without fat sat, so it should range from 0 to 1 in theory.

As seen in the B_0 maps, we picked two slices of the phantom that have relatively extreme off-resonance frequencies to demonstrate the principle. As seen in the last column in Figure 5, SLR fat sat did not suppress fat signal completely in regions with large off-resonance frequencies. SLR fat sat worked generally well for water parts, except for the edges where off-resonance frequencies are negative (last row), which is because the frequency response of the SLR pulse is asymmetric around the center frequency of water. In contrast, the FSMT-pulse worked more robustly for both water and fat in the presence of B_0 inhomogeneities. In addition, the FSMT-pulse is 58% shorter than the SLR fat sat pulse.

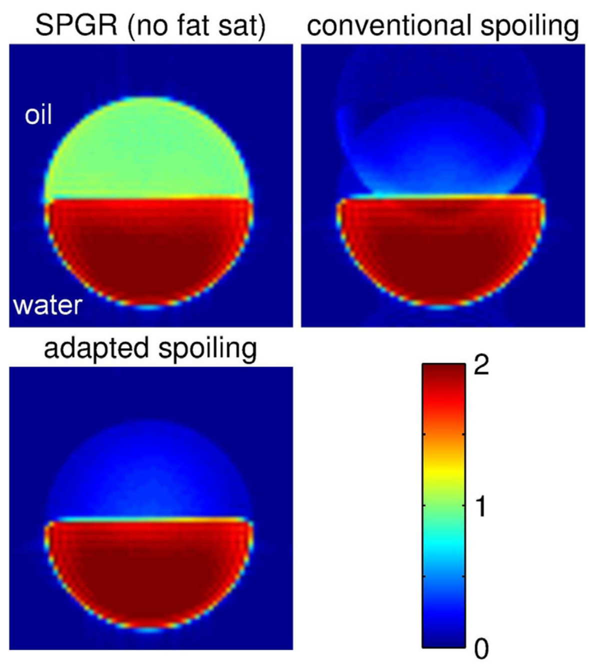

FIG. 4. An axial slice of the 3D SPGR images of the cylindrical phantom (oil on top of water) where all three images are at the same color scale: upper-left: fat sat off; upper-right: fat sat on with conventional RF spoiling; lower-left: fat sat on with adapted RF spoiling. The image with the conventional RF spoiling has ghosting artifacts due to data inconsistency, whereas the one with the adapted spoiling scheme is free of these artifacts.

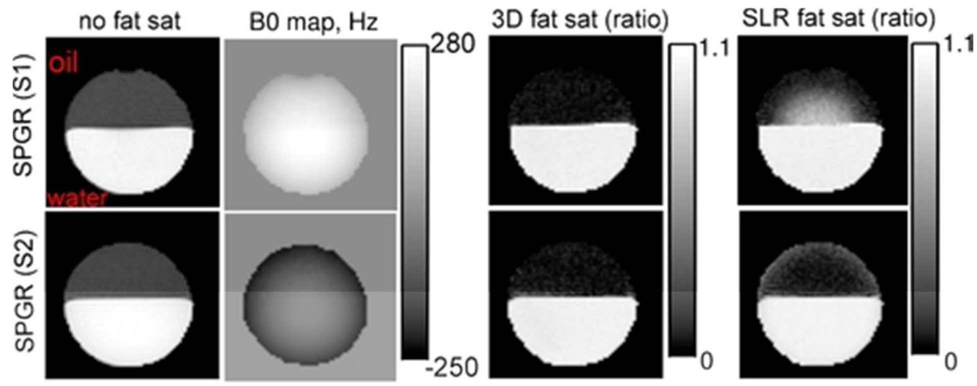

FIG. 5. The results of the phantom experiments for testing fat sat SPGR, where we picked two representative slices for each sequence. From left to right, first column: the original images with no fat sat (oil on top of water), second column: B_0 maps, third column: the ratio images with the 3D fat sat pulse, fourth column: the ratio images with the SLR fat sat pulse. The ratio image is calculated by taking the ratio between the image with fat sat and the corresponding image without fat sat.

Phantom Experiment III: Simultaneous Fat Sat and MTC Imaging

Figure 6 shows the B_0 map and the corresponding ratio images produced by FSMT-SPGR, where the ratio image is taken between the image with FSMT contrasts and the one without FSMT contrasts. The proposed sequence simultaneously suppressed fat and attenuated the MT phantom signal while the water signal maintains a similar level. By manually segmenting each image into the three parts, we calculated the average signal ratios of oil, water, and MT phantom, i.e., 0.076, 0.97, and 0.62, respectively. There may be some direct excitation of the FSMT-pulse to the MT phantom that can contribute to the attenuation in the MT phantom regions, and it is hard to separate this effect and MT effects. However, according to the simulation of the pulse (not shown), direct excitation in the MT phantom regions was very similar to direct excitation in the water regions. Since we observed very little direct excitation in the water regions, we believe the attenuation in the MT phantom regions were caused primarily by the MT effects from the FSMT-pulse.

In-Vivo Experiments I: Simultaneous Fat Sat and MTC Imaging in Brain

Figure 7 shows brain imaging results, where the proposed sequence effectively suppressed the fat tissue around the skull and optical nerves. In addition, white matter is significantly attenuated due to MT effects. As shown in the right image of Figure 7, the effective MTR in white matter is around 30% to 50%.

In-Vivo Experiments II: MRA in Brain

Figure 8 shows the results of the MRA experiment with the maximum intensity projections of the image with no FSMT-pulse (left) and with FSMT-pulse (right). Despite the presence of B_0 inhomogeneity, the FSMT-pulse greatly suppressed the fat tissue around the skull in the maximum intensity projections with FSMT contrasts, except that part of the fat around the left optical nerve was suppressed poorly due to large off-resonance effect (about 300 Hz). Furthermore, MT effects produced by the FSMT-pulse significantly reduced the background signals, and the arteries are better delineated in the maximum intensity projections compared to the one without FSMT contrasts, as pointed out by the red arrows. Those two images are each normalized to their own maximal intensity, because the blood signal was also attenuated due to its own MT effect and some direct excitation from the imperfect fat sat pulse, which is why the unsuppressed fat and optical nerve posterior to the left eye appears brighter in the FSMT contrast image. In addition, some veins, especially the ones anterior to the circle of Willis, are darker in the FSMT contrast image, because the FSMT-pulse, which was designed only for the imaging slab and the upstream region of the arteries,

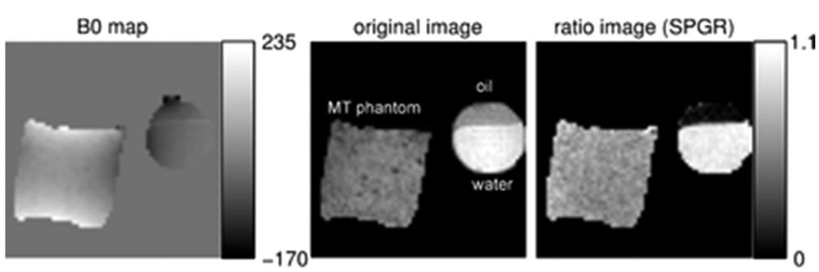

FIG. 6. The B_0 map and the resulting images of Phantom experiment III. Left: B_0 map in Hz; middle: the original SPGR image with FSMT disabled where oil, water, and the MT phantom are labeled; right: the ratio image taken between the one with FSMT contrast and the one without.

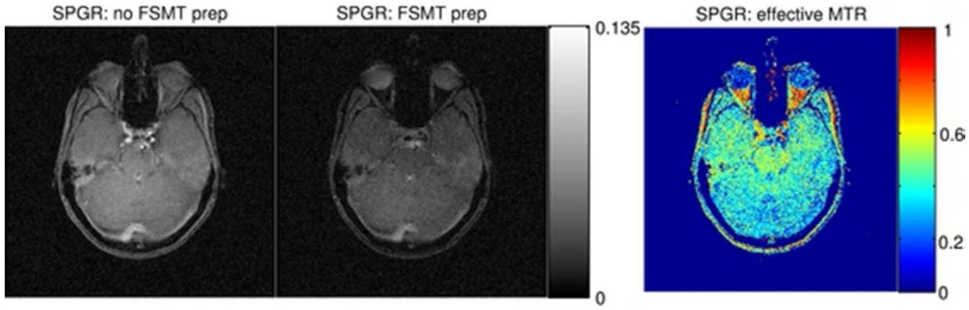

FIG. 7. SPGR images acquired in the in vivo experiments on human head. Left: without FSMT contrast; middle: with FSMT contrast; right: effective MTR maps. The left two images have the same gray scale.

may suppress the upstream regions of the veins. This feature may help reduce the need for vein suppression pulses. In general, the proposed FSMT-SPGR sequence improved the time-of-flight MRA in the brain by simultaneously suppressing fat and background tissue.

DISCUSSION AND CONCLUSIONS

In addition to the proposed FSMT SPGR sequence, we also show studies of the proposed FSMT STFR sequence in the Supporting Information. We proposed to apply the FSMT-pulse to SSI sequences, e.g., SPGR and STFR, to simultaneously do fat suppression and MTC. We demonstrated that an adapted RF spoiling scheme is required for fat sat SSI sequences to reach steady state. Compared to the conventional SLR fat sat, the FSMT-pulse is more robust to field inhomogeneity, and it can additionally produce MTC with SSI sequences having high sensitivity to magnetization attenuation. Examples of cartilage imaging (in Supporting Information) and brain MRA show that the proposed FSMT-SSI sequences can produce images that appear to be better for clinical use.

B_1 inhomogeneity could be ignored in our 3T experiments, but there are cases where B_1 inhomogeneity can be a potential issue, e.g., breast imaging (20). Then, the FSMT-pulse can help to compensate for B_1 inhomogeneity or even use parallel excitation (2), requiring B_1 mapping (21–23). This is another advantage over the conventional SLR fat sat. Although global specific absorption rate was kept below the limit in our experiments, local specific absorption rate penalty may be problematic when parallel excitation is used. Moreover, MT effects by the parallel excitation version of the FSMT-pulse may need further investigation.

We used 2D SSI sequences with 3D FSMT-pulse in most of the experiments. If a volumetric scan is needed, one may either do 3D imaging with 4D FSMT-pulse as used in the MRA experiment, or do 2D imaging slice by slice in a noninterleaved way. For the latter approach, the FSMT-pulses need to be designed for each slice individually based on multislice or 3D B_0 map. Comparing the MT effects of these two approaches, 4D FSMT-pulse is slightly longer than 3D FSMT-pulse, which is 2.5 ms versus 2.3 or 2.1 ms, but the 4D FSMT-pulse usually has similar or even higher energy, because it typically traverses the origin of the excitation k-space more densely than the 3D FSMT-pulse.

One advantage of SSI sequences over balanced steady-state free precession sequence for MTC imaging is that MTC SSI sequences can adjust the amplitude of MT effects more easily. The proposed sequences can adjust MT effects by changing the RF power constraints in the

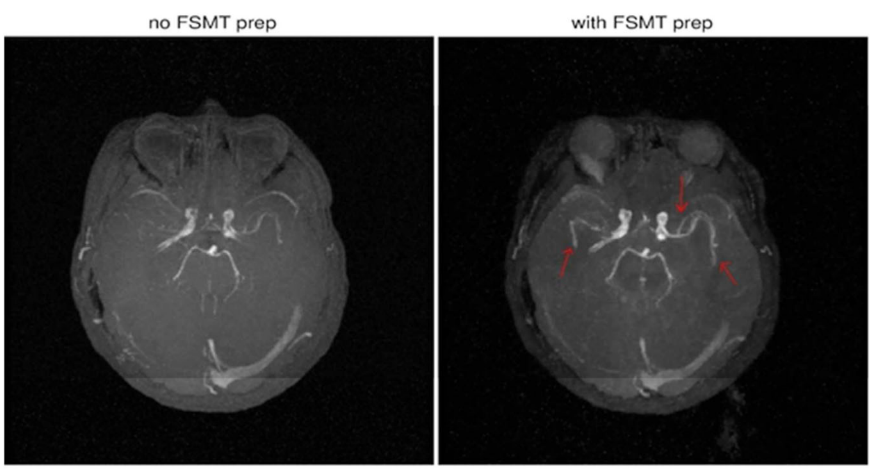

FIG. 8. The results of the MRA experiment where the maximum intensity projections with no FSMT contrast is on the left and the one with FSMT contrast on the right. Red arrows point to the arteries that are better delineated.

pulse design, e.g., by adjusting the corresponding regularization parameter. In our experiments, the RF energy of the FSMT-pulse could be reduced by up to 5–10 times with acceptable degradation in fat suppression performance, which may have very minimal MT effects. Thus, the proposed sequences with RF power penalization can potentially be used for applications that need only fat suppression.

Furthermore, it would be interesting to investigate the proposed sequences in more clinical applications that can benefit from fat suppression and MTC, e.g., cardiac imaging and breast imaging. Furthermore, as (2) has pointed out other potential benefits and issues of the FSMT-pulse at other field strengths than 3T, future work may include studies of the proposed sequences at those non-3T field strengths.

ACKNOWLEDGMENT

The authors would like to thank Hao Sun from The University of Michigan for useful discussions on RF spoiling, Luis Hernandez-Garcia from The University of Michigan for help on MRA experiments, and Vikas Gulani from Case Western Reserve University for suggestions on clinical applications.

APPENDIX

This appendix derives (1). Referring to Figure 1, we calculate the magnetizations at certain time points and each repetition of the sequence is segmented at those time points:

$$\overrightarrow{M}_1 \rightarrow P_1 \rightarrow \overrightarrow{M}_2 \rightarrow \text{free precession and } C_2 \rightarrow \overrightarrow{M}_3 \rightarrow S_1 \rightarrow \overrightarrow{M}_4$$

where

$$\overrightarrow{M}_1 = \begin{bmatrix} 0 \\ 0 \\ M_z \end{bmatrix}, \overrightarrow{M}_2 = \begin{bmatrix} 0 \\ M_z \sin\alpha \\ M_z \cos\alpha \end{bmatrix}$$

After the free precession and C_1, we have

$$\overrightarrow{M}_3 = \begin{bmatrix} 0 \\ 0 \\ \overrightarrow{M}_2(3)E_{1d} + (1 - E_{1d})M_0 \end{bmatrix}$$

In the MT part, i.e., S_1, the overall effect is a change in longitudinal magnetization followed by T_1 relaxation during C_2. Therefore, we have

$$\overrightarrow{M}_4 = \begin{bmatrix} 0 \\ 0 \\ (1 - \mathrm{MTR})\overrightarrow{M}_3(3)E_{1s} + (1 - E_{1s})M_0 \end{bmatrix}$$

When the sequence reach a steady state, we have $\overrightarrow{M}_4 = \overrightarrow{M}_1$ or $\overrightarrow{M}_4(3) = M_z$. Then, the steady-state longitudinal magnetization of MTC SPGR prior to each P_1 can be expressed as a function of MTR, which is equation (1).

REFERENCES

1. Haase A, Frahm J, Hanicke W, Matthaei D. 1H NMR chemical shift selective (CHESS) imaging. Phys Med Biol 1985;30:341–344.
2. Zhao F, Nielsen JF, Noll DC. Four dimensional spectral-spatial fat saturation pulse design. Magn Reson Med 2014;72:1637–1647.
3. Ozsarlak O, Van Goethem JW, Maes M, Parizel PM. MR angiography of the intracranial vessels: technical aspects and clinical applications. Neuroradiology 2004;46:955–972.
4. Adler J, Swanson SD, Schmiedlin-Ren P, Higgins PD, Golembeski CP, Polydorides AD, McKenna BJ, Hussain HK, Verrot TM, Zimmermann EM. Magnetization transfer helps detect intestinal fibrosis in an animal model of crohn disease. Radiology 2011;259:127–135.
5. Schmierer K, Scaravilli F, Altmann DR, Barker GJ, Miller DH. Magnetization transfer ratio and myelin in postmortem multiple sclerosis brain. Ann Neurol 2004;56:407–415.
6. Li D, Paschal C, Haacke E, Adler L. Coronary arteries: three-dimensional MR imaging with fat saturation and magnetization transfer contrast. Radiology 1993;187:401–406.
7. Flame DP, Pierce WB, Harms SE, Griffey RH. Magnetization transfer contrast in fat-suppressed steady-state three-dimensional MR images. Magn Reson Med 1992;26:122–131.
8. Wolff SD, Chesnick S, Frank J, Lim K, Balaban R. Magnetization transfer contrast: MR imaging of the knee. Radiology 1991;179:623–628.
9. Santyr GE, Kelcz F, Schneider E. Pulsed magnetization transfer contrast for MR imaging with application to breast. J Magn Reson Imaging 1996;6:203–212.
10. Jakob PM, Wang T, Schultz G, Hebestreit H, Hebestreit A, Elfeber M, Hahn D, Haase A. Magnetization transfer short inversion time inversion recovery enhanced 1H MRI of the human lung. Magn Reson Mater Phys Biol Med 2002;15:10–17.
11. Haacke EM, Brown RW, Thompson MR, Venkatesan R. Magnetic resonance imaging: physical principles and sequence design, Vol. 1. New York, Wiley-Liss, 1999.
12. Nielsen JF, Yoon D, Noll DC. Small-tip fast recovery imaging using non-slice-selective tailored tip-up pulses and radiofrequency-spoiling. Magn Reson Med 2013;69:657–666.
13. Sun H, Fessler JA, Noll DC, Nielsen JF. Steady-state functional MRI using spoiled small-tip fast recovery imaging. Magn Reson Med 2015; 73:536–543.
14. Zhao F, Nielsen JF, Noll DC. Fat saturation for 2D small-tip fast recovery imaging using tailored 3D spectral-spatial pulses. In Proceedings of the 21th Annual Meeting of ISMRM, Salt Lake City, Utah, USA, 2013. p. 252.
15. Zhao F, Swanson SD, Nielsen JF, Fessler JA, Noll DC. Simultaneous fat saturation and magnetization transfer preparation with 2D small-tip fast recovery imaging. In Proceedings of the 21th Annual Meeting of ISMRM, Salt Lake City, Utah, USA, 2013. p. 2507.
16. Henkelman RM, Huang X, Xiang QS, Stanisz G, Swanson SD, Bronskill MJ. Quantitative interpretation of magnetization transfer. Magn Reson Med 1993;29:759–766.
17. Zur Y, Wood M, Neuringer L. Spoiling of transverse magnetization in steady-state sequences. Magn Reson Med 1991;21:251–263.
18. Pauly J, Le Roux P, Nishimura D, Macovski A. Parameter relations for the Shinnar-Le Roux selective excitation pulse design algorithm. IEEE Trans Med Imaging 1991;10:53–65.
19. Malik SJ, Keihaninejad S, Hammers A, Hajnal JV. Tailored excitation in 3D with spiral nonselective (spins) RF pulses. Magn Reson Med 2012;67:1303–1315.
20. Kuhl CK, Kooijman H, Gieseke J, Schild HH. Effect of b1 inhomogeneity on breast MR imaging at 3.0 t. Radiology 2007;244:929–930.
21. Zhao F, Fessler J, Nielsen JF, Noll D. Regularized estimation of magnitude and phase of multiple-coil B1 field via Bloch-Siegert B1 mapping. In Proceedings of the 20th Annual Meeting of ISMRM, Melbourne, Australia, 2012. p. 2512.
22. Zhao F, Fessler JA, Wright SM, Rispoli JV, Noll DC. Optimized linear combinations of channels for complex multiple-coil B1 field estimation with Bloch-Siegert B1 mapping in MRI. In IEEE International Symposium on Biomedical Imaging: From Nano to Macro, San Francisco, California, USA, 2013. pp. 942–945.
23. Zhao F, Fessler J, Wright S, Noll D. Regularized estimation of magnitude and phase of multi-coil B1 field via Bloch-siegert B1 mapping and coil combination optimizations. IEEE Trans Med Imaging 2014. doi: 10.1109/TMI.2014.2329751.

Supplementary Material

Simultaneous Fat Saturation and Magnetization Transfer Contrast Imaging with Steady-State Incoherent Sequences

FENG ZHAO*,[1], JON-FREDRIK NIELSEN[1], SCOTT D. SWANSON[2], JEFFREY A. FESSLER[3] AND DOUGLAS C. NOLL[1]

[1]Biomedical Engineering Department, [2] Radiology Department, and [3] Department of Electrical Engineering and Computer Science, The University of Michigan, Ann Arbor, MI, USA

INTRODUCTION

This is the supplementary material for the paper "Simultaneous Fat Saturation and Magnetization Transfer Contrast Imaging with Steady-State Incoherent Sequences". In this material, we study the proposed fat sat and MT contrast applied to another SSI sequence, i.e., STFR. The following material starts with a brief overview of the original STFR sequence, and then we discuss the RF spoiling properies and MT contrasts of the proposed FSMT-STFR. Lastly, we demonstrate the proposed methods with simulation studies, phantom experiments and *in-vivo* experiments.

THEORY

Overview of STFR

Figure S-1 shows the proposed FSMT STFR sequence. The original STFR sequence proposed in (1) is the same excluding the FSMT-pulse part (P_0). Compared to SPGR, the main difference of STFR is the tailored tip-up pulse (P_2) at the end of each repetition; this tip-up pulse is tailored to tip up the excited spins back to the longitudinal axis, according to local off-resonance frequencies (1). By adding to the tip-up pulse to restore transverse magnetization, STFR produces high SNR T_2/T_1 contrast images. Another difference of STFR from SPGR is that its net gradient areas between the tip-down excitation and the tip-up pulse have to be zero, so that the spin behaviors are more controllable by the tip-up pulse.

SPGR and STFR have similar RF spoiling properties. For the regular STFR without fat sat, as the net gradient areas in between P_1 and P_2 are zero, the whole part that contains P_1 and P_2 can be treated as a single pulse from the RF spoiling's point of view. Thus, STFR works with the same RF spoiling scheme as SPGR when P_2 keeps the same global RF phase as P_1 (1).

With an additional gradient crusher (P_0) in each repeition, fat sat STFR using the conventional RF spoiling is guaranteed to reach steady state only with perfect fat sat, which is similar to fat sat SPGR. In addition, if P_2 and the nD fat sat pulse are not designed for the whole object, the uncontrolled out-of-slice/slab parts of the object can also produce non-steady-state signals (2). As STFR works with the same RF spoiling when keeping the global phase for P_1 and P_2, we proposed the same adapted RF spoiling scheme for fat sat STFR, and the functions of the global phase of each pulse in STFR also follow the equation [2] in the main paper.

Simultaneous Fat Sat and MTC imaging

Similar to the MT effect sensitivity study for SPGR, we can show that STFR with a MT pulse applied in each repetition also has higher MT effects than using the turbo type MT prep. With the same definitions of MTR and effective MTR as in the main paper, the Appendix of this supplmentary material derives the corresponding function of MTC STFR with respect to MTR:

$$M_z(\mathsf{MTR}) = M_0 \frac{[(1-\mathsf{MTR})E_{1s}^2(1-E_{1f})\cos\alpha + (1+(1-\mathsf{MTR})E_{1s})(1-E_{1s})]}{1-(1-\mathsf{MTR})E_{1s}^2(E_{2f}\sin^2\alpha - E_{1f}\cos^2\alpha)} \qquad \text{[S-1]}$$

where M_0 is equilibrium magnetization, $E_{1s} \triangleq e^{-\frac{T_s}{T_1}}$, T_s is the duration of each gradient crusher, $E_{1f} \triangleq e^{-\frac{T_f}{T_1}}$, $E_{2f} \triangleq e^{-\frac{T_f}{T_2}}$, T_f is the duration between the peak of P_1 and the beginning of P_2, α is the flip angle, and relaxation during tip-up and MT pulse is ignored.

Similar to Fig. 2, Fig. S-2 shows the MT contrast property of MTC STFR. The curves in Fig. S-2 correspond to the same range of T_1 and T_2 values used in Fig. 2, and the sequence was simulated with $T_s = 1$ ms and $T_f = 8$ ms. It is clear that MTC STFR with MT pulses applied in each repetition are much more efficient in producing MT effects than the corresponding turbo MT prep sequence. Such MT sensitivity increases with shorter T_R or longer T_1 and does not change much with different T_2 values. With this property and the same argument for FSMT-SPGR, we proposed to apply the FSMT-pulse to STFR to produce fat suppression and MT contrast simultaneously, which is called FSMT-STFR sequence.

METHODS AND RESULTS

Simulation: RF Spoiling Schemes

We first show a simulation study on the RF spoiling scheme for fat sat STFR. The simulation setup and parameters were kept the exactly same as the the simulation for SPGR. Fig. S-3 shows the signal evolutions of fat or water when fat-sat STFR is applied with the conventional RF spoiling scheme or the adapted RF spoiling scheme. In all the plots, the sequence with the conventional RF spoiling scheme can not reach steady state (blue solid lines), but the one with the adapted RF spoiling scheme reaches steady state after 100 repetitions at most (red dashed lines).

Phantom Experiment: Fat Sat Pulses

Corresponding to Phantom Experiment II for SPGR, we applied FSMT STFR with the same experiment setup to the same object. It was also compared with the same 5 ms SLR fat sat pulse. According to the corresponding B_0 maps respectively, we designed 2.1 ms long FSMT-pulses with 5 repetitions of 2D spiral-out excitation k-space trajectories, as well as the 2D tailored tip-up pulses (P_2 in Fig. S-1). The adapted RF spoiling scheme was applied to all the sequences. The imaging parameters were kept the same except that T_R were 4.9 ms longer than the corresponding SPGR sequences respectively.

Fig. S-4 shows the results of the experiments, which in general show similar comparison between the FSMT-pulse and the SLR fat sat compared to the results in Fig. 5 for FSMT SPGR. Note that STFR images are less uniform in the oil parts, because the tailored tip-up pulses were designed only for water and have off-resonance effects on fat, making fat suppression more important in STFR imaging. Moreover, although the B_0 maps of these experiments are similar to those of the SPGR experiments, SPGR with SLR fat sat worked well enough for water in both slices, which shows that the fat-sat SPGR is less sensitive to water selection from fat sat pulse than the fat-sat STFR with these particular parameters and object materials .

In-Vivo Experiment: Brain Imaging

Similar to the *in-vivo* experiment I for SPGR, we tested the proposed FSMT-STFR with a brain imaging experiment at 3T. The FSMT-pulse was 2.3 ms long with 7 repetitions of 2D spiral-out trajectories. Using the same experiment setup as for FSMT-SPGR , we applied FSMT-STFR at a superior axial brain slice. The imaging parameters of the STFR sequence were kept the same as in the SPGR experiment except that T_R was 19.1 ms. Fig. S-5 shows the results of this experiment, where FSMT-SPGR suppresses the fat tissue around skulls and attenuates the white matter regions. Specifically, white matter signal is reduced by 50% - 70%.

In-Vivo Experiment: Cartilage Imaging

We then investigated the proposed sequence in the application of cartilage imaging where contrast between synovial fluid and cartilage is desired. Fat suppression is generally beneficial to this application because it can eliminate the surrounding fat that would obscure the tissue of interest (3)(4). MTC is useful for T_2 weighted (5) or T_2/T_1 weighted cartilage imaging (3), where synovial fluid appears brighter than cartilage, so MT can enhance the fluid-cartilage contrast by attenuating cartilage signals.

Therefore, we applied the proposed FSMT-STFR which produces T_2/T_1 contrast (1) to cartilage imaging in human knees. 2D STFR with FSMT-pulse is designed for an axial slice based on a 2D B_0 map acquired with SPGR sequences, and the image data were acquired with 2D spin-warp readout. The FSMT-pulse was 2.1 ms long using 7 repetitions of spiral-out trajectories. One additional image was taken with the FSMT-pulse off as the reference. Other imaging parameters were: slice thickness $= 6$ mm, T_R is 18.5 ms, flip angle $= 16^0$, $a = 117^0$, 1.09 mm$\times 1.09$ mm resolution, FOV = 28 cm $\times 14$ cm.

Fig. S-6 shows the cartilage imaging results comparing the image with no FSMT contrast (middle) to the one with FSMT contrast by the FSMT-pulse (bottom), and the corresponding B_0 map is shown at the top. Fat suppression removed the fat tissue surrounding the cartilage and joint fluid areas and also helped removing the posterior fat that has artifacts due to the tailored tip-up pulse of STFR. In particular, the FSMT-pulse worked very well in the regions with large B_0 inhomogeneity, such as the posterior fat regions. In addition, MT effects suppressed cartilage and muscle signals, and thus highlighted the synovial fluid signals which are pointed out by the red arrows.

APPENDIX

This appendix supplements detailed derivation for equation [S-1]. Referring to Fig.S-1, we calculate the magnetizations at certain time points and each repetition of the sequence is segmented at those time points:

$$\vec{M}_1 \rightarrow P_1 \rightarrow \vec{M}_2 \rightarrow \text{free precession} \rightarrow \vec{M}_3 \rightarrow P_2 \rightarrow \vec{M}_4 \rightarrow C_2 \rightarrow \vec{M}_5 \rightarrow S_1 \rightarrow \vec{M}_6$$

where

$$\vec{M}_1 = \begin{bmatrix} 0 \\ 0 \\ M_z \end{bmatrix}, \vec{M}_2 = \begin{bmatrix} 0 \\ M_z \sin\alpha \\ M_z \cos\alpha \end{bmatrix}$$

After the free precession, there are spin relaxation effects and off-resonance effects, leading to:

$$\vec{M}_3 = \begin{bmatrix} \cos\phi & \sin\phi & 0 \\ -\sin\phi & \cos\phi & 0 \\ 0 & 0 & 1 \end{bmatrix} \begin{bmatrix} \vec{M}_2(1)E_{2f} \\ \vec{M}_2(1)E_{2f} \\ \vec{M}_2(3)E_{1f} \end{bmatrix} + \begin{bmatrix} 0 \\ 0 \\ (1-E_{1f})M_0 \end{bmatrix}$$

where ϕ denotes the phase accumulated due off-resonance effects. If we assume the tip-up pulse is perfectly designed to revert off-resonance effects during the free precession and also have tip-up angle α towards the longitudinal axis, then we have:

$$\vec{M}_4 = \begin{bmatrix} \cos\phi & \sin\phi & 0 \\ -\sin\phi & \cos\phi & 0 \\ 0 & 0 & 1 \end{bmatrix} \begin{bmatrix} 1 & 0 & 0 \\ 0 & \cos\alpha & -\sin\alpha \\ 0 & \sin\alpha & \cos\alpha \end{bmatrix} \begin{bmatrix} \cos\phi & -\sin\phi & 0 \\ \sin\phi & \cos\phi & 0 \\ 0 & 0 & 1 \end{bmatrix} \vec{M}_3$$

Then if the crusher C_2 perfectly removes the transverse magnetization, we then have:

$$\vec{M}_4 = \begin{bmatrix} 0 \\ 0 \\ E_{1s}\vec{M}_4(3) + (1-E_{1s})M_0 \end{bmatrix}$$

After C_2, we consider the overall effect of S_1 as having a change in the z magnetization due to MTR and T_1 relaxation. Hence, we have:

$$\vec{M}_6 = \begin{bmatrix} 0 \\ 0 \\ (1 - \text{MTR})\vec{M}_5(3)E_{1s} + (1 - E_{1s})M_0 \end{bmatrix}$$

When the sequence reach a steady state, we have $\vec{M}_6 = \vec{M}_1$ or $\vec{M}_6(3) = M_z$. Then the steady-state longitudinal magnetization of MTC STFR prior to each P_1 can be expressed as a function of MTR, which is equation [S-1].

References

1. Nielsen JF, Yoon D, Noll DC. Small-tip fast recovery imaging using non-slice-selective tailored tip-up pulses and radiofrequency-spoiling. Magnetic Resonance in Medicine 2013;69:657–666.

2. Zhao F, Nielsen JF, Noll DC. Fat saturation for 2D small-tip fast recovery imaging using tailored 3D spectral-spatial pulses. In Proceedings of the 21th Scientific Meeting of International Society for Magnetic Resonance in Medicine, Salt Lake City. 2013; 252.

3. Gold GE, Reeder SB, Yu H, Kornaat P, Shimakawa AS, Johnson JW, Pelc NJ, Beaulieu CF, Brittain JH. Articular cartilage of the knee: Rapid three-dimensional MR imaging at 3.0 t with ideal balanced steady-state free precession—initial experience1. Radiology 2006;240:546–551.

4. Disler DG, McCauley TR, Wirth CR, Fuchs MD. Detection of knee hyaline cartilage defects using fat-suppressed three-dimensional spoiled gradient-echo mr imaging: comparison with standard mr imaging and correlation with arthroscopy. American journal of roentgenology 1995;165:377–382.

5. Lang P, Noorbakhsh F, Yoshioka H. Mr imaging of articular cartilage: current state and recent developments. Radiologic Clinics of North America 2005;43:629–639.

FIGURES

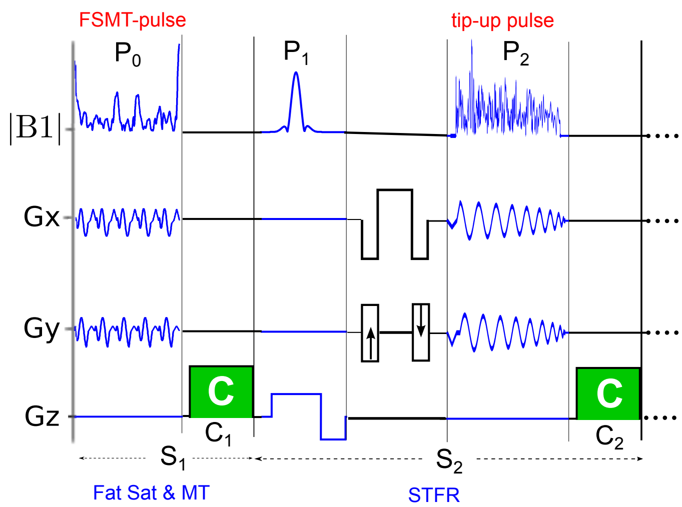

Figure S-1: Illustration of the 2D version of the proposed FSMT-STFR sequence.

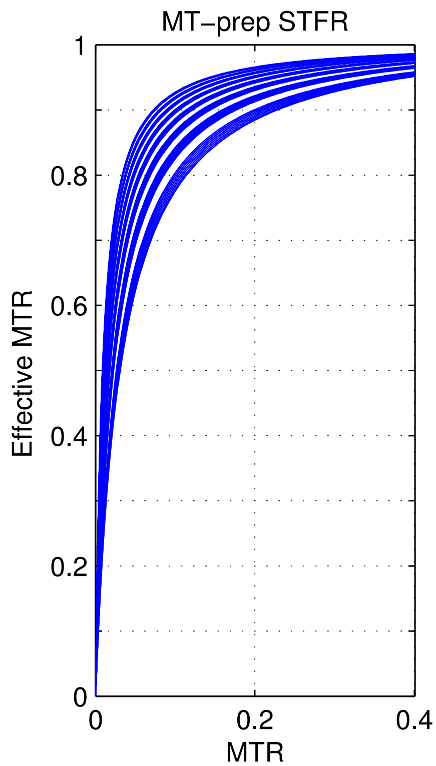

Figure S-2: Plots of the effective MTR in terms of MTR for MTC STFR; The plots are from all the combinations of the following relaxation parameters: $T_1 = [0.5, 0.7, \ldots, 1.7, 1.9]$ s, and $T_2 = [50, 70, \ldots, 170, 190]$ ms. STFR is sensitive to small magnetization attenuation caused by MT effect.

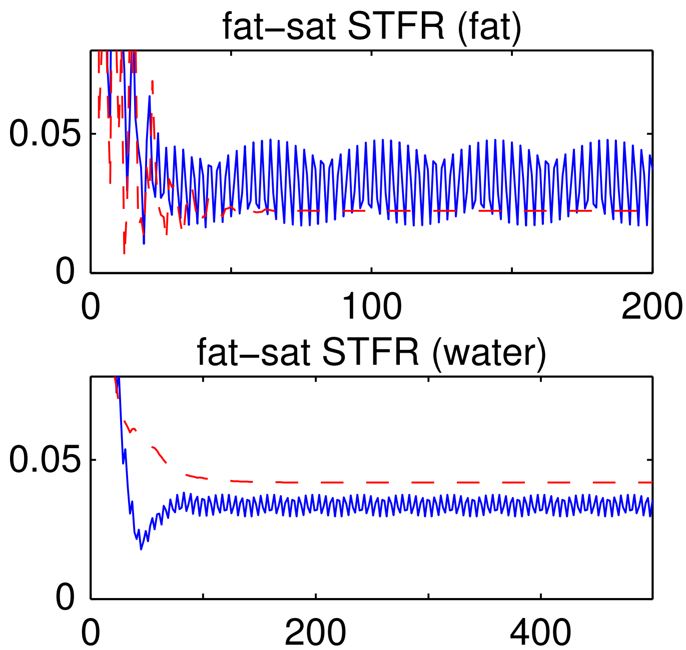

Figure S-3: Signal evolutions of fat spin (upper row) and water spin (lower row) using fat-sat STFR with different RF spoiling schemes. Both longitudinal axes denote the ratio between the transverse magnetization right after P_1 and the magnetization at equilibrium, M_{xy}/M_0; the horizontal axes denote the number of repetitions. The signal reaches steady state with the adapted RF spoiling scheme (dashed lines), but not with the conventional RF spoiling scheme (solid lines).

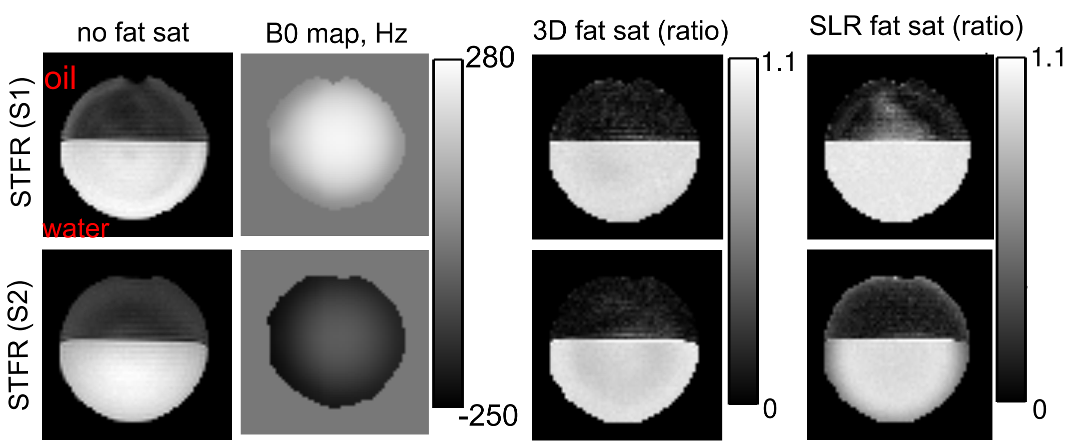

Figure S-4: The results of the phantom experiments for testing fat-sat STFR where we picked two representative slices for each sequence. From left to right, 1st column: the original images with no fat sat (oil on top of water), 2nd column: B_0 maps, 3rd column: the ratio images with the 3D fat sat pulse, 4th column: the ratio images with the SLR fat sat pulse. The ratio image is calculated by taking the ratio between the image with fat sat and the corresponding image without fat sat.

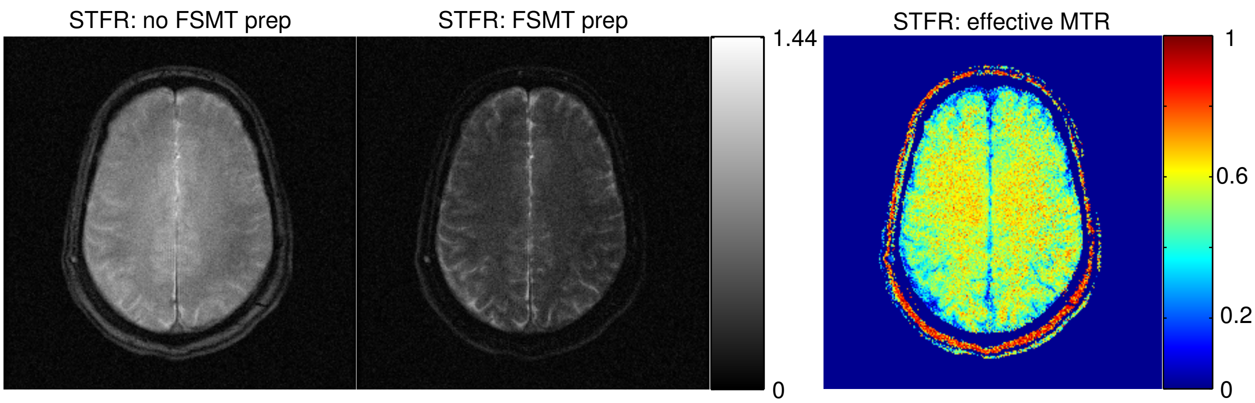

Figure S-5: STFR images acquired in the *in-vivo* experiments on human head. Left: without FSMT contrast; middle: with FSMT contrast; right: effective MTR maps. The left two images have the same gray scale.

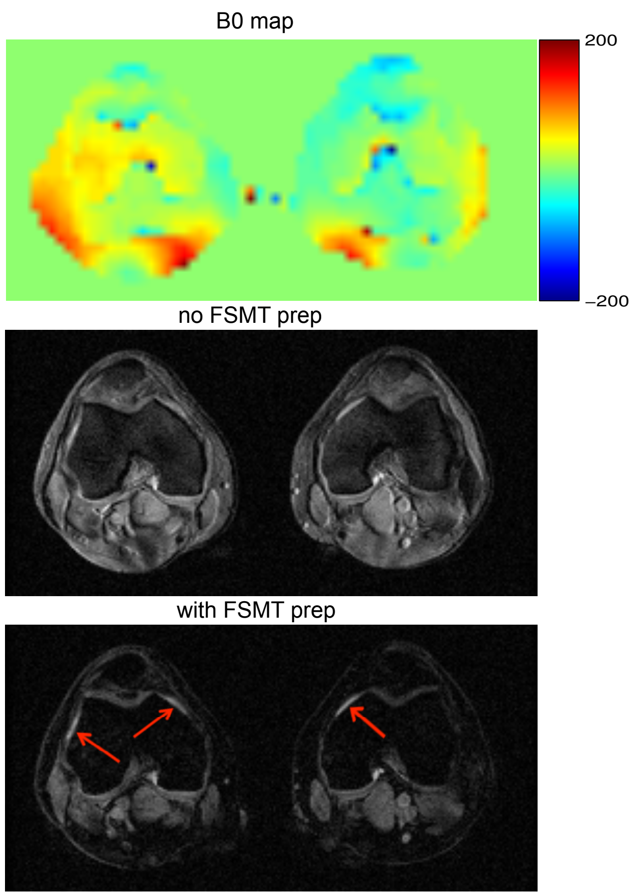

Figure S-6: The resulting STFR images of the cartilage imaging and the corresponding B_0 map (top). The image with no FSMT-pulse is at the middle, and the image with FSMT-pulse is at the bottom. These two images are in the same gray scale. The red arrows point to synovial fluid which is highlighted better in the image with simultaneous fat suppression and MTC.